physica status solidi

pss

www.pss-journals.com

reprint

WILEY-VCH

Phys. Status Solidi A **210**, No. 4, 658–668 (2013) / **DOI** 10.1002/pssa.201200532

Part of Special Issue on
Advanced Concepts for Silicon Based Photovoltaics

physica status solidi a
www.pss-a.com
applications and materials science

Characterization of a-SiN$_x$:H layer: Bulk properties, interface with Si and solar cell efficiency

Machteld Lamers[*,1], **Keith Butler**[2], **Per Erik Vullum**[3], **John Harding**[2], **and Arthur Weeber**[1]

[1] ECN Solar Energy, P.O. Box 1, 1755 ZG Petten, The Netherlands
[2] University of Sheffield, Western Bank, Sheffield S10 2TN, UK
[3] SINTEF, Box 4760 Sluppen, 7465 Trondheim, Norway

Received 27 July 2012, revised 30 October 2012, accepted 30 October 2012
Published online 29 November 2012

Keywords characterization, PECVD, silicon nitride, solar cells

* Corresponding author: e-mail lamers@ecn.nl, Phone: 31 88515 4718, Fax: 31 88515 8214

In this paper two front-side a-SiN$_x$:H layers that can be used in the solar cell industry are extensively characterized and related to solar cell efficiency. Variations in layer build up, atomic density, optical properties, bulk passivation and surface passivation are discussed. The build up of these two layers are considered against a background of over 80 SiN$_x$:H layers. These layers differ in stoichiometry, atomic content, optical properties and surface passivation, as the refractive index is varied between 1.8 and 3.0. Additionally, comparable data output of different characterization equipment is discussed on validity. On solar cells, the effect of different layer build up is investigated and it is found that a wide process window is allowed for similar cell efficiencies regarding the optical transmission, bulk and surface passivation.

© 2012 WILEY-VCH Verlag GmbH & Co. KGaA, Weinheim

1 Introduction Hydrogenated amorphous silicon nitride (a-SiN$_x$:H) is the standard antireflection and passivating layer, for both surface and bulk defects, in wafer-based silicon solar cells. Commonly, the layer is deposited using plasma-enhanced chemical vapour deposition (PECVD). The physical properties of the layer have previously been correlated to cell output properties like the open-circuit voltage V_{oc} [1, 2]. In general, the optimized a-SiN$_x$:H layer is a compromise between optical (antireflection and absorption) properties, and bulk and surface passivation. Si-rich a-SiN$_x$:H layers show good surface passivation, but are highly absorbing and cannot be used for solar cell applications. N-rich layers show good optical properties, but are less effective in surface passivation. Additionally, sufficient N–H bonds should be present in the layer as H released by breakage of this bond during the high temperature firing, causes bulk passivation [3–5]. In the literature, extensive characterization results can be found for different a-SiN$_x$:H layers deposited with various equipment [1, 4, 6, 7]. Commonly, the a-SiN$_x$:H layer is approximated by a homogeneous composition, *i.e.*, bond densities, optical properties and atomic density are found to be constant throughout the layer. However, variations in the layers do exist and can be small, which allow the layer to be characterized as homogeneous, or can be large, in which case the layer is inhomogeneous. In this article we provide a background data set in which over 80 a-SiN$_x$:H layers are characterized. Against this background homogeneous and inhomogeneous layers are compared using extensive characterization, also allowing the results using different characterization equipment to be compared. The effect of the build up of the layers is related to the three functions of a-SiN$_x$:H on solar cells: as anti-reflection coating and as provider for bulk passivation and surface passivation of the silicon wafer.

2 Setting the background

2.1 Sample preparation Samples were prepared using 275 μm thick p-type FZ <100> wafers and 500 μm thick p-type Cz <100> wafers, which were double side mirror polished with a base resistivity of 2.5 Ωcm and >20 Ωcm, respectively. Remote PECVD using the MAiA system of Roth and Rau [8] was used to deposit 80–110 nm a-SiN$_x$:H layers on the wafers. Variations in deposition were obtained by varying the pressure (0.1–0.5 mbar), temperature (275–475 °C), total gas flow (200–1250 sccm), plasma

© 2012 WILEY-VCH Verlag GmbH & Co. KGaA, Weinheim

power (400–3320 W) and gas ratio NH_3/SiH_4 (1–7). These parameters are identified as influencing the layer composition and are discussed in more detail in Ref. [9]. Before deposition, the wafers received a 1% HF dip. The Cz wafers were single side coated, while the FZ wafers were coated on both sides. The first were used for Fourier transform infrared spectroscopy (FTIR) and spectroscopic ellipsometry measurements. The latter were used to determine the minority charge carrier lifetime measurements using the Sinton Consulting WCT-120 lifetime tester [10]. Lifetime was determined at a minority carrier density of $1 \times 10^{15}\,cm^{-3}$. Surface recombination velocity (SRV) was determined from this value, taking into account the doping of the wafer [11]. FTIR bond densities were calculated from the spectrum using the conversion factors as found by Giorgis et al. [12]. It is noted that the values needed to convert the data from the FTIR spectrum to the bond density cannot be regarded as exact [6], but we believe they represent a good first approximation. Spectroscopic ellipsometry (280–820 nm) was performed at three angles of incidence (50°, 60° and 70°) and the layers were analysed using the Urban model. From the fit, the refractive index n and the extinction coefficient k were determined at respectively 633 nm and 400 nm. The formulation defined by Bustarret et al. [13] was used to calculate the Si-Si bond densities and atomic densities.

2.2 Optical properties, bond densities and surface passivation The ellipsometry data of the layers could be fitted well with a single layer model and the spectral trend for n and k were comparable to what is commonly observed [7]. This indicates that the layers have a homogeneous build up. In Figs. 1A and B the bond densities of the layers, determined using FTIR, as a function of n at 633 nm are given. This range in n corresponds to x in SiN_x:H from 1.45 to 0.15 as is shown in Fig. 1C. In this figure it can also be seen that k at 400 nm becomes zero for $x > 1.1$, which corresponds to $n < 2.03$.

It can be seen that the variation around the guideline of the Si–Si bond density is small, which can be expected as the Si–Si bond density is calculated from n. For $n < 3.0$ the Si–Si bond density increases almost linearly with increasing n. The Si–N bond density is constant for $n < 2.1$, but decreases linearly with increasing n. For low n, the Si–H bond density is negligible, but increases until $n = 2.4$–2.5, after which this bond density is stable. By contrast, the N–H bond density is high for layers with low n, but rapidly decreases with increasing n, with the maximum curvature around $n = 2.0$. A transition of the dominant bond from N–H to Si–H is found at $n = 2.0$ ($x = 1.15$), which is similar to the transition point as found in Ref. [14] and which has been identified as the percolation threshold of Si–Si bonds [15].

Using [13], the atomic densities can be calculated and from this, the total atomic density. In Fig. 2, the total atomic density is given for the layers made with the MAiA system. As can be seen, the density increases linearly with n, though the error is quite large.

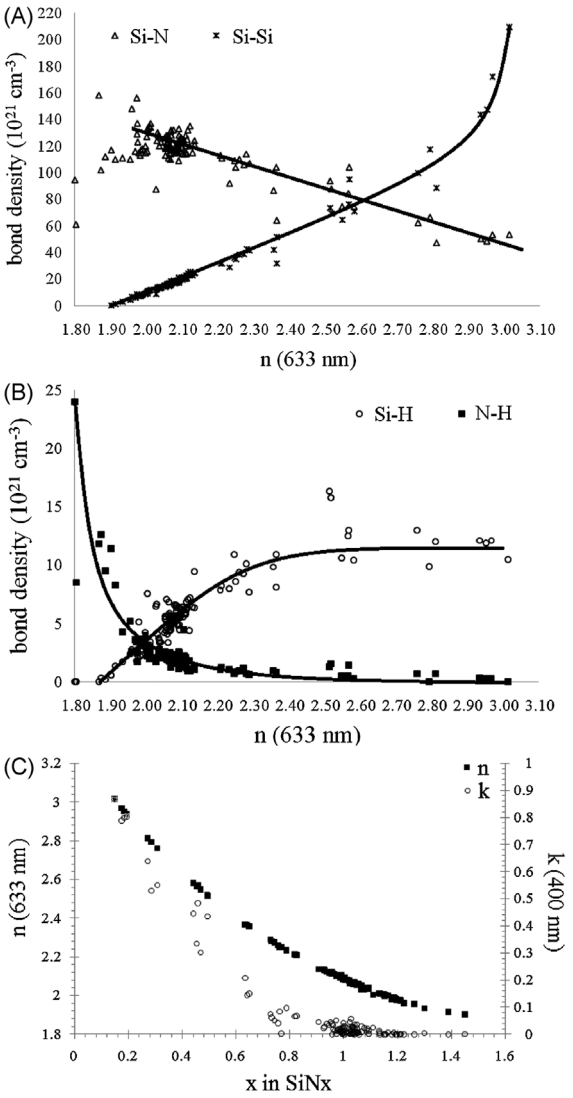

Figure 1 The Si–N and Si–Si bond densities (A) and Si–H and N–H bond densities (B) as function of n at 633 nm for over 80 a-SiN_x:H layers. The lines are guides to the eye. (C) The relationship between x in SiN_x:H and n at 633 nm and k at 400 nm.

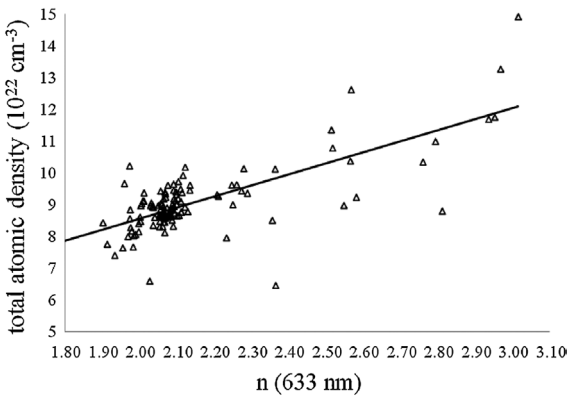

Figure 2 Total atomic density as function of n for the MAiA layers. The line is a guide to the eye.

© 2012 WILEY-VCH Verlag GmbH & Co. KGaA, Weinheim

From the data, the atomic percentage of H, Si and N as found in the layers is determined. They are given in Fig. 3A and B as a function of n and the extinction coefficient k. As can be seen and is expected, n correlates strongly with the Si and N atomic percentages, but is more or less independent of H. A minimum in H concentration can be seen around $n = 1.9$–2.0 as the N–H bond density rapidly decreases while the Si–H bond density increases much slower. At this point the main atomic bonding of H switches from N to Si. The minimum H percentage is around 5% while the maximum around 15%. It should also be noted that the total H concentration increases with n, as the total atomic density increases. Regarding k, this parameter becomes zero for $n < 2.03$, which corresponds to atomic percentage of Si $< 45\%$. However, at the transition point where the percentage of Si becomes larger than the percentage of N, k increases and increment linearly with larger percentages of Si.

In Fig. 4 the effective SRV as calculated from the lifetime is given as a function of n. The SRV is determined for the samples before and after the high temperature firing step, commonly used in solar cell manufacturing to realize the screen-printed metal contacts [16].

As can be seen, for low n the SRV is very high, but this drops quickly with increasing n. At around $n = 2.1$ low SRV values are obtained. The effective SRV remains stable for higher n. The variation between before and after firing cannot be fully linked to the firing process or firing stability of the layers, as no clear differences between before and after firing can be seen. Variations in the obtained effective SRV for similar n, can in detail be more specifically linked to the Si–H bond density of the specific layer. In Fig. 5 the Si–H bond density as function of the effective SRV is given for all layers with $2.0 < n < 2.15$.

In this section a background has been developed based on homogeneous layers. It is shown that with increasing n, the:

(i) Si–N bond density decreases linearly;
(ii) Si–Si bond density increases linearly;
(iii) N–H bond density declines very rapidly for $n < 2.1$; for $n > 2.1$, the decline rate reduces significantly and becomes linear;
(iv) Si–H bond density first increases linearly, but stabilizes for $n > 2.4$;
(v) Total density increases;
(vi) Si content increases linearly;
(vii) N content decreases linearly;
(viii) H content varies between 5 and 15% and shows a minimum at $n = 1.9$;

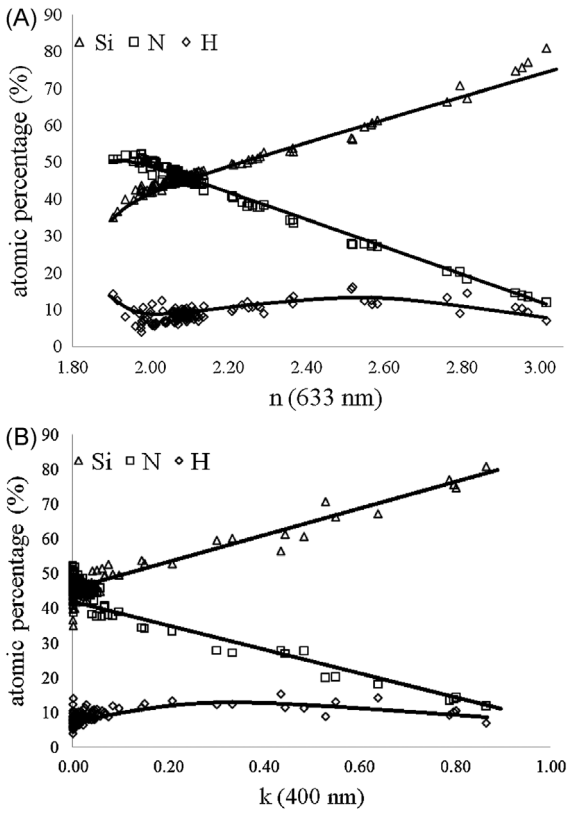

Figure 3 Atomic percentage of H, Si and N as function of n (A) and k (B). The lines are guides to the eye.

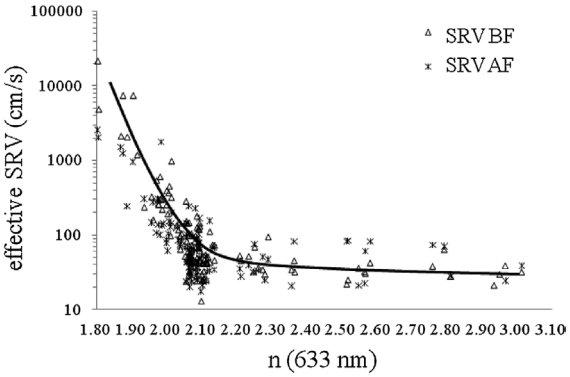

Figure 4 Effective SRV before (BF) and after firing (AF) as a function of n. The line is a guide to the eye.

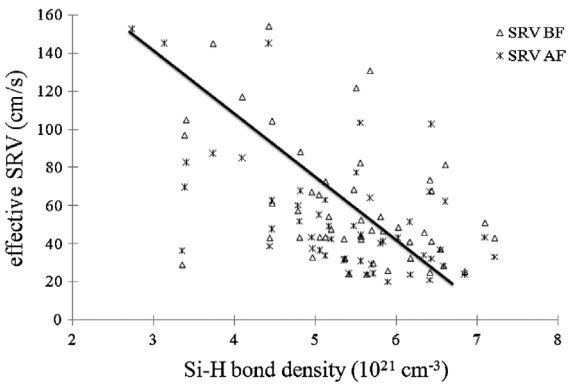

Figure 5 Effective SRV before (BF) and after firing (AF) as a function of the Si–H bond density for all layers with $2.0 < n < 2.15$. The line is a guide to the eye.

© 2012 WILEY-VCH Verlag GmbH & Co. KGaA, Weinheim

(ix) SRV is very high for low n, but start to stabilize and remain constant for $n > 2.1$.

3 Characterization accuracy

3.1 Homogeneity throughout the layer: atomic concentration measured by SIMS and FTIR/ellipsometry In the previous section the results from FTIR and ellipsometry were combined to obtain more insight into the layer build up and to obtain correlations between bonds, densities, atomic content, surface passivation and optical properties. In this characterization, a homogeneous build up of the layer is assumed. Variations in layer build up can have an effect on different properties, but are not considered in this approach. To study the layer build up in more detail, samples fabricated by two different PECVD systems, namely the MAiA and the SiNA (also from Roth and Rau) are analysed. Our SiNA system is a prototype and is described in more detail in Ref. [9]. The MAiA layers can be approached as homogeneous in layer build up, while the SiNA layers are inhomogeneous. Variations in layer build-up can be related to differences in gas flow distribution throughout the system. To compare homogeneous and inhomogeneous layers, for each type a passivating and standard a-SiN_x:H layer was fabricated and analysed in various ways. To analyse the variation of bond densities and optical properties in a more detailed manner, the two inhomogeneous layers are etched back in small steps. Each etch step consisted of a 2 min 9% HF dip, a 10 s 0.05% KOH dip and a 3 min 1% HCl dip. After each etch step the layers were analysed with lifetime measurements, FTIR and ellipsometry. For layers thinner than 15 nm the FTIR signal became weak, which limits the accuracy of the analysis of this data. Also, surface roughening due to the etch back process needs to be taken into account and can explain the variations around the line drawn in the figures.

The two layers analysed were optimized as a front side layer (standard a-SiN_x:H), with changing n from Si-side to air-side from 2.4 to 2.0 and as a surface passivating layer (passivating a-SiN_x:H), with changing n from Si-side to air-side from 2.8 to 2.4. The change in n for both layers is discussed in Section 3.3. The Si–N, Si–H bond densities and Si–H peak location as a function of the remaining layer thickness for the two back etched inhomogeneous layers are shown in Figs. 6–8.

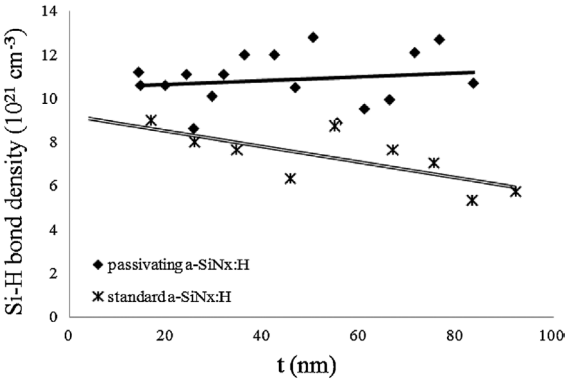

Figure 7 The Si–H bond density as a function of the remaining layer thickness t for the passivating and standard inhomogeneous layers.

The composition of the layer clearly changes. It can be seen that for the passivating layer a steep decrease in Si–N bond density is found, though the Si–H bond density and peak position remains stable. The relative composition of each part of the inhomogeneous layer follows very closely the atomic composition as found for the homogeneous layers shown in Fig. 3.

The H atomic concentration found for the investigated layers is compared to the calibrated H atomic concentration found by Time-of-Flight Secondary Ion Mass Spectroscopy (ToF-SIMS). For this, the bond densities needed to be calculated as function of the distance from the Si surface. A fit was made through the data points as shown in Figs. 6 and 7. Using this fit, the bond density as function of the distance could be calculated, using,

$$[X-Y] = \frac{d_e[X-Y]_e - d_{e+1}[X-Y]_{e+1}}{d_e - d_{e+1}}, \quad (1)$$

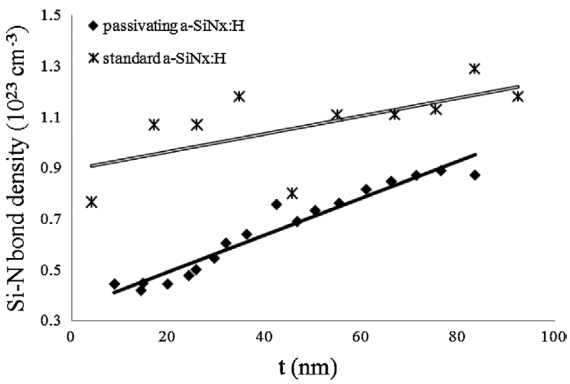

Figure 6 The Si–N bond density as a function of the remaining layer thickness t for the passivating and standard inhomogeneous layers.

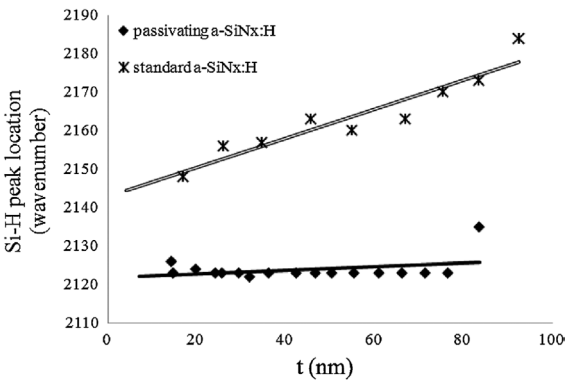

Figure 8 The Si–H peak location as a function of the remaining layer thickness t for the passivating and standard inhomogeneous layers.

© 2012 WILEY-VCH Verlag GmbH & Co. KGaA, Weinheim

where $[X-Y]$ representing the bond density like Si–H or Si–N as function of the distance from the Si surface; $[X-Y]_e$ the measured integral value of the bond density after etch step number e; $[X-Y]_{e+1}$ the measured integral value of the bond density after etch step number $e+1$; d_e the thickness of the layer after etch step number e; d_{e+1} the thickness of the layer after etch step $e+1$.

The results for H are shown in Fig. 9.

As can be seen, the H concentrations determined by ToF-SIMS and FTIR/ellipsometry are comparable. The variation throughout the layer in the inhomogeneous passivating layer is not large. This is as expected, as layers with low effective SRV ($n > 2.4$), even though fluctuating in n ($n = 2.4$–2.8), will give similar densities of Si–H bonds and hence similar H concentrations. The inhomogeneous standard layer, with $n = 2.0$–2.4 is expected to give a larger variation in H concentration and this is also found. Even more, the layers exhibit quite a high H concentration between 5 and 20 nm from the Si interface, corresponding to 11% of the total atomic density within in the layer. The homogeneous layer shows indeed on *average* a constant H profile. On closer examination variations in the layer can be observed suggesting a small change in composition at half thickness. This small variation can be related to the presence of two PECVD sources in the machine and the movement of the tray underneath these sources. The small variation occurs as the deposition is done at the boundary area of the two plasmas.

Also, the ^{29}SiN and ^{30}Si peak signals of the ToF-SIMS data are further investigated. An estimation of the Si density in a-SiN$_x$:H can be obtained by relating the average ^{30}Si signal of the c-Si bulk to the density of c-Si (2.329 g cm^{-3}) and using this ratio to estimate the Si density in the a-SiN$_x$:H layer. The Si density as determined by ToF-SIMS and FTIR/ellipsometry is shown in Fig. 10.

As can be seen, the (uncalibrated) Si concentration determined by ToF-SIMS does not follow the same trend as the Si concentration determined by FTIR/ellipsometry, and also the absolute values differ. However, both measurements give a higher Si concentration for the passivating inhomogeneous layer than for the standard inhomogeneous layer, conforming to expectations. Also, a large increasing trend is found in Si in the inhomogeneous standard layer, moving towards the Si interface. The homogeneous layer shows a very constant Si concentration, except for a small peak at half thickness. The three layers show different behaviour close to the interface and this can be related to matrix effects of SIMS measurements.

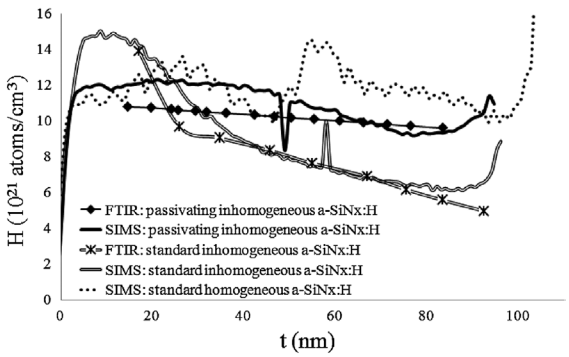

Figure 9 The H concentration in the standard homogeneous layer and passivating and standard inhomogeneous layers.

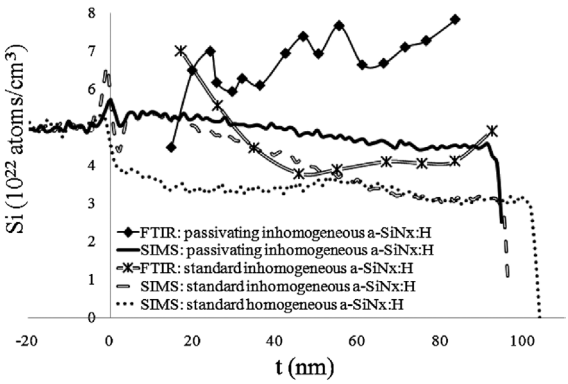

Figure 10 The Si concentration in the standard homogeneous layer and passivating and standard inhomogeneous layers.

The ^{29}SiN signal divided by the average ^{30}Si signal in bulk c-Si gives a profile of the Si–N bond density in the a-SiN$_x$:H. The ^{29}SiN/^{30}Si(c-Si bulk) signal as determined from the ToF-SIMS data is shown in Fig. 11.

As can be seen the intensity of ^{29}SiN/^{30}Si(c-Si) is quite similar for all samples. For the inhomogeneous passivating layer a decrease in ^{29}SiN is found, as expected, as n increases simultaneously. While the homogeneous standard layer gives a constant value on *average*, clear but small variations in data can be seen. The inhomogeneous standard layer at first shows an increase, followed by a decrease in ^{29}SiN. Comparing Fig. 11 with Fig. 6, it can be seen that the reduction in N is similar for the inhomogeneous passivating a-SiN$_x$:H layer, but is quite different for the inhomogeneous standard a-SiN$_x$:H layer.

Comparison of two different analysis methods shows a comparable (calibrated) H content for different a-SiN$_x$:H

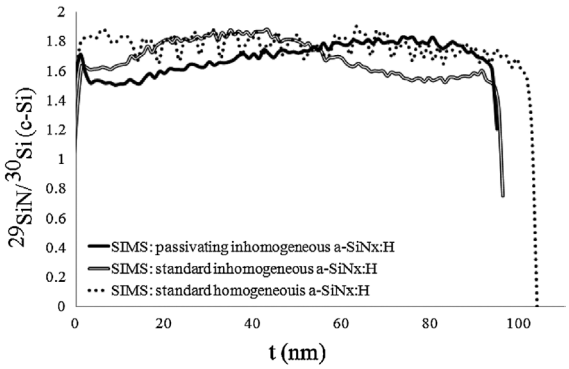

Figure 11 The ^{29}SiN/^{30}Si (c-Si bulk) signal of the standard homogeneous layer and passivating and standard inhomogeneous layers.

© 2012 WILEY-VCH Verlag GmbH & Co. KGaA, Weinheim

methods, though quite a different conclusion related to Si. In the next section two additional different methods to determine the exact Si and N content are used to analyse the layers and discuss the results in more detail.

Regarding the comparison between homogeneous and inhomogeneous layers an initial conclusion can be made that variations in layer build-up occur for all the layers. However, in homogeneous layers the variations are relatively small and the composition is *on average* constant. In inhomogeneous layers similar variations can be found, however a clear trend is observed in these variations.

3.2 Homogeneity throughout the layer: atomic concentration measured by XPS, TEM and FTIR/ellipsometry To examine the exact Si and N content further, the inhomogeneous standard layer was characterized with X-ray photoelectron spectroscopy (XPS) and transmission electron microscopy (TEM). The analyses were performed at SINTEF. The XPS measurements were performed using Al Kα radiation ($h\nu = 1486.6$ eV) combined with Ar^+ sputtering (2 keV, 1 mm^2 raster size) for depth profiling. Cross-section TEM specimens were prepared by mechanical polishing, dimpling and Ar^+-ion sputtering using liquid nitrogen to cool the sample. The acceleration voltage was progressively reduced to 1.0 keV during the final stage of the Ar^+-ion sputtering to minimize sample damage. TEM was performed with a JEOL 2010F operated at 200 kV. Compositional analysis was performed with X-ray energy dispersive spectroscopy (EDS) using a 0.5 nm in diameter electron beam.

In Fig. 12 the atomic percentage (including only Si and N) as found by XPS, TEM and FTIR/ellipsometry are given for the inhomogeneous standard layer.

As can be seen in the graph, the TEM underestimates the N concentration, which is a known problem when characterizing low mass atoms. The trend however follows the SIMS profile, indicating that the underestimation is constant. The percentages as measured by XPS and FTIR/ellipsometry found for both Si and N are similar. Closer to the Si interface the values deviate. Though the general trend is similar, for a significant increase in Si content, the FTIR/ellipsometry data gives a faster increase, while the increase in percentage is higher for the XPS data. The behaviour of the XPS can be explained by the resolution of the measurements. Close to the Si surface this surface is incorporated in the analysis, hence effectively increasing the Si content. Furthermore, in XPS, depth is determined by etching speed and is assumed to be constant throughout the sample, which is not valid for a sample with inhomogeneous build up. To confirm this hypothesis the passivating inhomogeneous sample was also analysed by XPS and these results, along with the FTIR/ellipsometry data and are shown in Fig. 13.

Also in this comparison it can be seen that the atomic percentages as found by XPS and FTIR/ellipsometry are relatively close when far from the Si interface, but when close to this surface the Si content drastically increases. Moreover, 15–20 nm from the interface no N is found in the layer, which indicates that the material should be a-Si:H. This is highly unlikely as, both FTIR, ellipsometry and ToF-SIMS contradict this. Also, the surface passivation of this layer is stable under firing, and does not deteriorate as expected for real a-Si:H layers, which should crystallize during the firing step. Therefore, a depth error is present in the XPS analyses of the layer. However, from the data obtained far from the interface it can be concluded that the atomic percentages as found by FTIR/ellipsometry and XPS match.

Analyses of a-SiN_x:H layers by TEM, ToF-SIMS, XPS, FTIR and ellipsometry show a variation in the estimated Si, N and H content throughout the a-SiN_x:H layer. Variations within the layers themselves exist and can be identified, however accurate quantification is difficult as the error can be quite large.

3.3 Homogeneity throughout the layer: optical properties as determined by ellipsometry and reflection To maximize the short circuit current J_{sc} of a solar cell, the a-SiN_x:H layer should not absorb light and minimize reflection to allow maximum transmission. For this reason, we examine in more detail the ellipsometry data and compare this to the spectral reflection as measured using an integrating sphere. For the homogeneous layers the

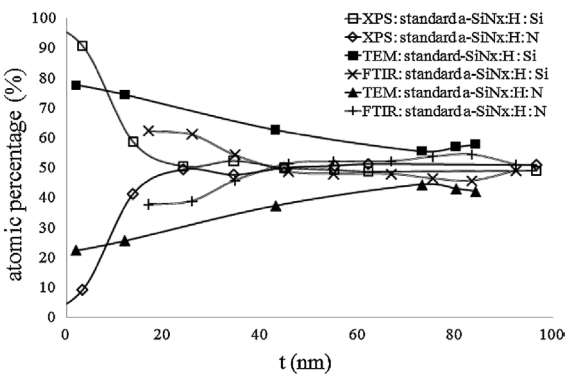

Figure 12 The Si and N atomic percentages in the inhomogeneous standard layer, characterized by XPS, TEM and FTIR/ellipsometry.

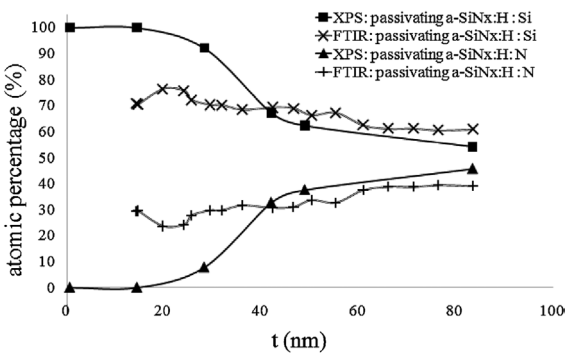

Figure 13 The Si and N atomic percentages in the inhomogeneous passivating layer, characterized by XPS and FTIR/ellipsometry.

© 2012 WILEY-VCH Verlag GmbH & Co. KGaA, Weinheim

measured reflection matched closely the reflection simulated using the optical properties modelled using ellipsometry data (not shown). However, the reflection of the inhomogeneous layers is more complicated as the variation in the layer build up determines the reflection. In Fig. 14 the refractive index n, the extinction coefficient k of two layers, a passivating and standard layer, are given as a function of the thickness t. Two approaches were used in the fitting of the ellipsometry data. The first is the modelling of the full layer as a two-stack layer. The second is by modelling the last etched layer first and adding an additional layer on top, building the a-SiN$_x$:H layer as such. It can be seen that a higher n and k is found for the passivating layer relative to the standard layer. With both models, a clear increase in n and k can be seen throughout the layers. A drop in both n and k is present for almost completely etched layers. This can be related to the oxidation of the already exposed Si surface in the back-etching process, which interferes with the analysis. Also, this drop might also be related to the presence of native oxide grown on the Si surface after the 1% HF dip, as was confirmed by ToF-SIMS.

In Fig. 15 the reflections of the passivating and two-stack layers are shown. Additionally the calculated reflections based on the ellipsometry measurements are given. As can be seen the fitted reflection matches the measured data well. This leads to the conclusion that similar reflection curves can be obtained for layers with similar thicknesses though the internal variation in n and k can change. Also, this leads to the conclusion that n and k calculations based on the reflection curves can lead to different values and should be seen as an average, rather than the exact value of that layer.

Thus, the measured effective reflection, relevant for solar cells, is dependent on the *average* behaviour within the layer and not on small deviations within the layer.

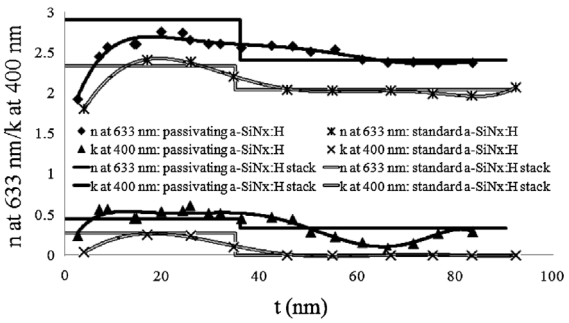

Figure 14 n and k as determined at 633 and 400 nm, respectively, as a function of t for the passivating and the standard a-SiN$_x$:H layer. Two methods are used to fit the data with ellipsometry: the etch back and a two-stack layer.

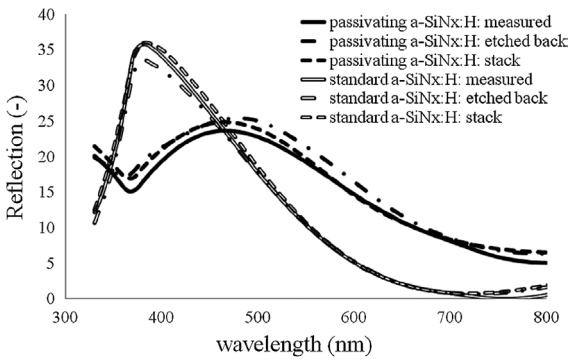

Figure 15 The measured reflection of the two a-SiN$_x$:H layers. Also the calculated reflection based on the data from ellipsometry is given.

4 Passivation The a-SiN$_x$:H layer passivates both the bulk and the surface of a Si wafer. The first can be understood as the release of H from the a-SiN$_x$:H layer, which diffuses into the Si bulk where it passivates defects. The latter can be understood as the reduction of dangling bonds at the surface of the Si wafer and the repulsion of the holes in the Si wafer by the positive fixed charges (Q_f) at the a-SiN$_x$:H/Si interface, thereby reducing recombination. The former is called a reduction of the density of interface states (D_{it}); the latter field effect passivation. In this section these aspects and characterization of passivation is investigated.

4.1 Bulk passivation Bulk passivation has been identified as caused by the release of H atoms during the high temperature firing step as N–H bonds break [3–5]. The atomic H diffuses through the a-SiN$_x$:H and Si layers and bonds to defects it encounters, thereby passivating them. Logically, layers with a high N–H density will release more H than layers with hardly any N–H. As can be seen in Fig. 1B the former layer correspond to layers with low n, the latter correspond to layers with high n. Also, the layers with low n have a lower total density than layers with a high n (Fig. 2). However, in layers with low density and high N–H density, the atomic H can easily form H_2, which is released to the outside world, thereby effectively reducing the amount of atomic H in the layer [4] and the V_{oc} of the solar cell. An optimum has been found for layers with a Si–N bond density between 1.2 and 1.3×10^{23} cm^{-3} [1]. The effect on solar cells significantly depends on the bulk quality of the Si wafer, *i.e.* the amount of defects to be passivated. For high Si–N bond density (and low N–H bond density) the atomic H released from the layers is too little to passivate defects in Si, thereby effectively reducing the V_{oc} [1].

4.2 Surface passivation As Q_f and D_{it} are properties of the interface of a-SiN$_x$:H/Si, this indicates that they are determined by the initial growth of the a-SiN$_x$:H layer. More profoundly, Q_f is related to the interface structure between the materials (a-SiN$_x$:H and Si) causing a local-field effect as was described by Aspnes [17]. The origin of Q_f is linked to the so-called K- and N-centres [15, 18]. These centres are respectively *Si=N$_3$ and *N=Si$_2$. * indicates that these centres can be neutral, positive, negative or bonded to H. Assuming that K- and N-centres also occur at the interface, this leads to the conclusion that Q_f is determined by the variation and volume fractions of K- and N-centres at the

© 2012 WILEY-VCH Verlag GmbH & Co. KGaA, Weinheim

interface region of a-SiN$_x$:H/Si. The number of K-centres that are bonded to H can be calculated from the Si–H peak in a FTIR spectrum [12]. A peak location close to 2220 cm^{-1} indicates relatively more K-centres. Both the K- and N-centres have also been suggested as the origins of the dangling bonds at the interface and therefore related to D_{it}. Therefore, when the concentration of (charged) K- and/or N-centres increases, Q_f becomes larger. Simultaneously, as the volume fraction of the centres is increased, the amount of (unpassivated) dangling bonds also increases and so D_{it} increases as well.

Selected homogeneous layers of the background data set were further analysed. The peaks in the FTIR spectrum were deconvoluted to find the specific back bonds of the Si–H and Si–N peaks. The literature on the exact values needed to convert the area of the FTIR spectrum per bond to a density is not conclusive; we decided to show the data in terms of peak area of the bond density [6]. On both sides of the samples with single side a-SiN$_x$:H a 300 nm aluminium single layer was deposited to create metal-insulator-silicon (MIS) structures. Q_f and D_{it} were determined using capacitance-voltage (CV) MIS analysis. The relationships between the deconvoluted Si–H bond density in the H–Si–N$_3$ configuration (at 2220 cm^{-1}), the total Si–H bond density, the N–H bond density, the deconvoluted Si–N bond density in the locally distorted configuration (at 790 cm^{-1}) and the refractive index n (at 633 nm as determined with ellipsometry) are shown in Fig. 16 [19].

Again the relationships between the Si–N, Si–H and N–H bond densities are shown, as given in Fig. 1A and B. It can be seen that the H–Si–N$_3$ bond and the Si–N bond in locally distorted configuration follow the same trend, with an optimum around $n = 2.3$.

The relationships between the effective SRV, Q_f, D_{it} and the refractive index n (at 633 nm as determined with ellipsometry) are shown in Fig. 17.

The Q_f found in our experiments is relatively high. To confirm the validity of the results, a comparison was done

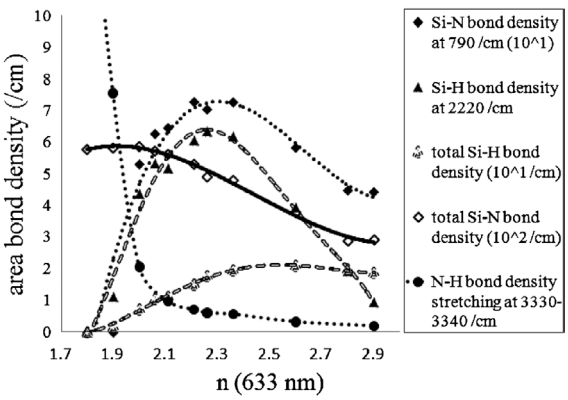

Figure 16 Relationship between (the peak areas of) the Si–H bond density, the deconvoluted Si–H bond density at 2220 cm^{-1}, the Si–N bond density, the deconvoluted Si–N bond density at 790 cm^{-1} (distorted), N–H bond density and n [19].

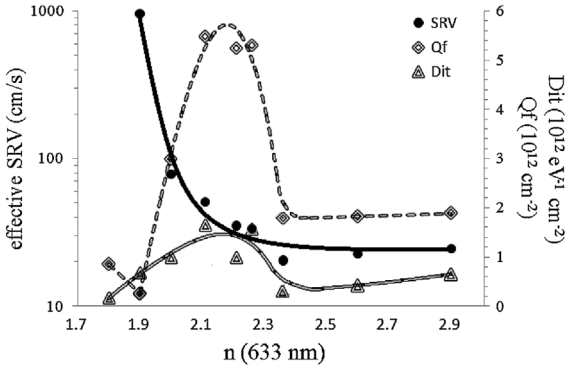

Figure 17 Relationship between the effective SRV, Q_f and n. The lines are guides to the eye.

with SiN$_x$:H fabricated with a batch PECVD, which showed similar values as obtained in Ref. [20]. Also, reference Al_2O_3 layers were measured and comparative values were obtained.

A clear and positive correlation between Q_f and D_{it} is found. Furthermore, at low n, the Q_f is nearly absent and the effective SRV is determined by the (high) D_{it}. In Fig. 16 it is seen that in these layers the H-bonded K-centre is not present and distortion inside the layer is very low. With increasing n and decreasing SRV, Q_f and D_{it} increase as well, just like the H-bonded K-centres and distortion. This can be explained since, as the number of charged K-centres increases, the neutral dangling bonds (uncharged and non-passivated K-centres) increase as well. With even higher n, and low SRV, Q_f and D_{it} decrease again to a certain level, simultaneous with a drop in H-bonded K-centres and distortion in the layer. The effective SRV is a combined effect of Q_f and passivation of dangling Si bonds by H (high Si–H bond density) [19, 21]. The latter relation is depicted in Fig. 15.

Molecular dynamics (MD) simulations of the interface were performed at the University of Sheffield using de Brito Mota's [22] parameterization of the Tersoff potential [23]. The bonding patterns are found to depend on the stoichiometry of the system and increasing defective geometries and distortion correspond to the presence of K- and N-centres. This correlates with the increased presence of K- and N-centres at the interface as shown in Fig. 16. Since charge carriers barely penetrate into the a-SiN$_x$:H region only the defect centres at the surface will be expected to affect the recombination rates. The modelling methods and results are described in more detail in Refs. [24, 25].

For inhomogeneous layers a correlation between the bulk properties and surface passivation is more complicated as the composition of the layer changes. To identify which part of the a-SiN$_x$:H layer determines the surface passivation, the standard and passivating layers have been back etched and lifetime measurements are performed after each etch step. The results are given in Fig. 18.

As can be seen, the lifetime, and thus surface passivation, remains constant even for very thin layers. For the standard

© 2012 WILEY-VCH Verlag GmbH & Co. KGaA, Weinheim

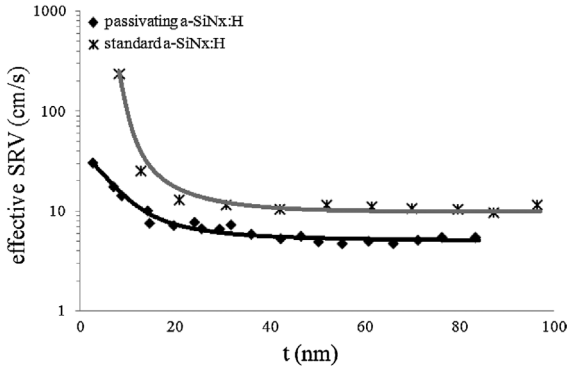

Figure 18 The effective SRV at 10^{15} cm^{-3} measured as a function of the distance to the Si surface. The lines are guides to the eye.

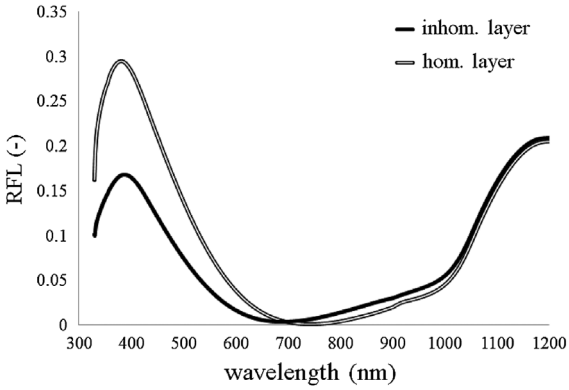

Figure 19 Reflection (RFL) of a mc-Si cell (excluding reflection from metallization) fabricated with an inhomogeneous and homogeneous a-SiN$_x$:H coating.

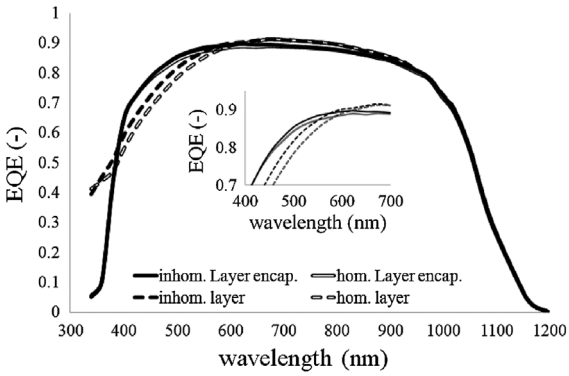

Figure 20 EQE before and after encapsulation of mc-Si cells fabricated with an inhomogeneous and homogeneous a-SiN$_x$:H coating.

layer the lifetime drops even for a relatively thick layer, but this might be due to inhomogeneous etching, as the etch rate for the standard layer is much higher than for passivating a-SiN$_x$:H. This indicates that the location of Q_f is very close to the interface.

5 Solar cells Thus far, we have shown the results of an extended investigation into a-SiN$_x$:H layers. Different aspects have come forward in analysing different layers, especially when obvious inhomogeneities in the layer build up are present. In this section the effect on p-type solar cells of these different layers is investigated. The wafers were 180 μm thick with a base doping of 1–2 Ωcm, sized 156×156 mm^2. The process flow used is described in Ref. [16].

5.1 Light management: reflection, absorption and transmission For optimal light management of a solar cell coated with a homogeneous standard layer, the refractive index should be around 2.05 [26, 27]. For this n, absorption in the layer is negligible and transmission at optimum thickness is maximal. Fabrication of a stack layer, to reduce further the optical losses, can lead to higher J_{sc}. However, after encapsulation this difference becomes much smaller. Also, absorption by the a-SiN$_x$:H layer with increasing n decreases J_{sc}. To illustrate this, two p-type mc-Si cells are fabricated, one with the homogeneous standard layer, the other with the inhomogeneous layer. The reflection of these cells, corrected for the reflection losses by the front side metallization, is given in Fig. 19.

As can be seen in the figure a clear difference is found in the reflection. The inhomogeneous layer has absorption, determined by analysing the ellipsometry data, which lowers the transmission. Also, for the homogeneous layer the reflection minimum is at too high wavelength, which decreases J_{sc} (fabrication error). On the cell level the external quantum efficiency (EQE) is significantly higher for the inhomogeneous layer, while this difference reduces significantly after encapsulation in EVA and glass. The EQE is shown in Fig. 20. The difference still present after encapsulation is mainly related to the difference in reflection minimum.

These results indicate significant differences in reflection, and even more, significant variations in layer build up, have minimal effect on solar cells after encapsulation.

In Table 1, the averaged solar cell parameters of 5 cells are given for two material qualities and for both a-SiN$_x$:H layers. The difference in material quality was obtained by selecting material from both the bottom (“better”) and the middle (“lower”) of an ingot, which result in differences in impurities which effect cell efficiency [28]. Comparing the two different a-SiN$_x$:H layers, the main difference is in the J_{sc}, which can be explained by the difference in reflection minimum. The difference in V_{oc} is explained in Section 5.3.

5.2 Bulk passivation: low versus good wafer quality Solar cell efficiency is to a large extent determined by the wafer quality and thus by the properties of a-SiN$_x$:H to passivate defects in the bulk. As discussed in Section 4.1, for excellent bulk passivation, the optimum Si–N bond density should be $1.2–1.3 \times 10^{23}$ cm^{-3}. For the homogeneous layer the N–H bonds are distributed evenly throughout the layer, whereas for the inhomogeneous a-SiN$_x$:H, the higher density of N–H bonds is found closer to the outer surface. To validate

© 2012 WILEY-VCH Verlag GmbH & Co. KGaA, Weinheim

Table 1 Average solar cell parameters of five cells using both lower and better material quality for two types of a-SiN_x:H layers.

layer	wafer quality	J_{sc} (mA cm^{-2})	V_{oc} (mV)	FF (%)	efficiency (%)
inhomogeneous	better	35.1	612	77.6	16.74
	lower	35.2	610	77.4	16.57
homogeneous	better	34.7	610	77.4	16.38
	lower	34.7	608	77.4	16.34

whether sufficient atomic H can reach the bulk Si, mc-Si cells were processed in four groups: three different homogeneous standard layers and one inhomogeneous layer were tested. Each group contained five wafers of lower and five wafers of better wafer quality, neighbouring to the wafers discussed in Section 5.1 and also the same process flow was used. In Fig. 21, two different box plots are shown, one representing the cell data for the lower quality material, the other representing the data for the better quality material. The V_{oc}–V_{oc}(max) is shown as a function of the average Si–N bond density of the layers; V_{oc}(max) is the maximum V_{oc} found in the cells processed per a-SiN_x:H group.

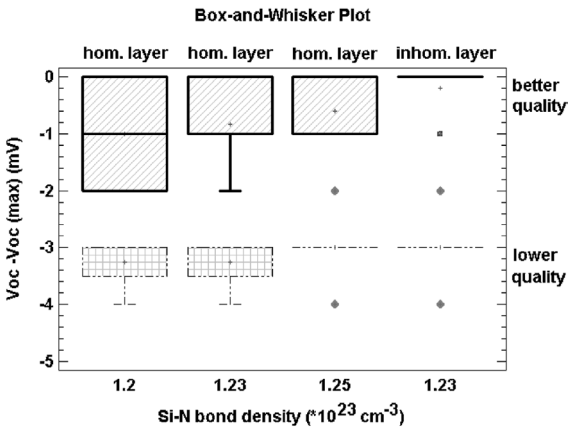

Figure 21 The V_{oc}–V_{oc} (max) for inhomogeneous and homogeneous a-SiN_x:H layers as function of the average Si–N bond density of the layers.

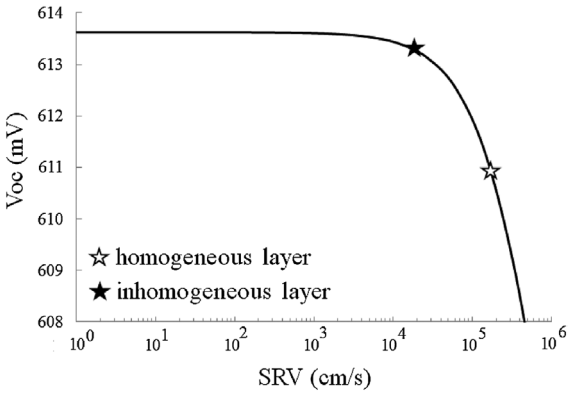

Figure 22 The V_{oc} as function of SRV as modelled with PC1D. In the plot two points are given for the experimental data of the inhomogeneous and homogeneous layer.

No statistical difference is found, *i.e.*, the difference in V_{oc} between better and lower wafer quality is similar for all groups. As bulk passivation is determined by the N–H bonds, these results indicate that the position (or spread) of the N–H bonds in the layer is not of importance. This is accordance with Boehme, who stated that the reduction of H during the dissociation processes is homogeneous throughout the film since any density gradient is instantly compensated for because of the high diffusivity of H [29].

5.3 Surface passivation In a phosphorus emitter the amount of minority carriers (holes) that are to be repelled from the surface is low, due to the field effect passivation of and the high recombination rate in the emitter. The SRV of the emitter itself was determined by Cuevas et al. [30] and for a standard high doped emitter, the effective SRV is between 10^4 and 10^5 cm s^{-1}. The inhomogeneous and homogeneous standard a-SiN_x:H layers give a different effective SRV on <100> DSP FZ, 30 and 60 cm s^{-1}, respectively, which is a significant difference in surface passivation. On the p-type cell level, this corresponds to a difference in 2–3 mV on average of more than 100 cells of both better and lower mc-Si quality and Cz material. The cells are modelled in PC1D [31] and the effect on V_{oc} as function of the effective SRV is shown in Fig. 22, the experimentally obtained V_{oc} are also shown.

In the figure the V_{oc}, obtained from PC1D modelling of the p-type mc-Si cell, is given as a function of the front surface recombination SRV. A strong dependency can be found for SRV $>1 \times 10^4$ cm s^{-1}, which is the region of the effective emitter recombination. The difference in V_{oc} for the two layers correspond to the difference is surface passivation. The effect of Q_f is further described in Ref. [1].

6 Conclusions Over 80 a-SiN_x:H layers are analysed using FTIR, ellipsometry and QSSPC lifetime measurements to find a well defined composition build up of the layer for homogeneous layers. Clear correlations are found between optical properties n and k and the bulk properties like the Si–Si, Si–H, N–H and Si–N bonds and interface properties like Q_f and D_{it}. The real homogeneity throughout both apparently homogeneous and inhomogeneous layers is investigated using FTIR, ellipsometry, ToF-SIMS, TEM and XPS. The outcome of using the different characterization equipment is compared and discussed. The effects of both homogeneous and inhomogeneous layers on solar cell efficiency are compared. It was found that small deviations in the layer do not have a large influence, but large

© 2012 WILEY-VCH Verlag GmbH & Co. KGaA, Weinheim

variations in the composition will. It is also shown that reflection differences, giving a significant effect on cell level, can become insignificant after encapsulation. Bulk passivation for standard mc-Si solar cells is influenced by the N–H bond density and total mass density, but it is shown that the exact location of the N–H bond in the layer is not critical. Surface passivation depends strongly on the composition of the a-SiN$_x$:H close to the interface and it is shown that differences in surface passivation can influence the V_{oc} of the solar cell. A difference of 2 mV was found.

The effective differences in solar cells performance, when encapsulated, for different a-SiN$_x$:H layers, are relative small and give an indication of the wide process window for the a-SiN$_x$:H layers on the front side of solar cells.

Acknowledgements The authors acknowledge support from the European Commission grant MMP3-SL-2009-228513, "Hipersol" as part of the 7th Framework Package, grant number 228513. Via our membership of the UK's HPC Materials Chemistry Consortium, which is funded by EPSRC (EP/F067496), this work made use of the facilities of HECToR, the UK's national high-performance computing service, which is provided by UoE HPCx Ltd at the University of Edinburgh, Cray Inc and NAG Ltd, and funded by the Office of Science and Technology through EPSRC's High End Computing Programme.

References

[1] I. G. Romijn, W. J. Soppe, H. C. Rieffe, A. R. Burgers, and A. W. Weeber, in: Proc. 20th European Photovoltaic Solar Energy Conference and Exhibition, Barcelona, Spain, 2005, p. 1352.
[2] H. F. W. Dekkers, L. Carnel, G. Beaucarne, and W. Beyer, in: Proc. 20th European Photovoltaic Solar Energy Conference and Exhibition, Barcelona, Spain, 2005, p. 721.
[3] J. Hong, W. M. M. Kessels, F. J. H. van Assche, H. C. Rieffe, W. J. Soppe, A. W. Weeber, and M. C. M. van de Sanden, Prog. Photovolt.: Res. Appl. **11**, 125 (2001).
[4] H. F. W. Dekkers, in: Study and Optimization of Dry Process Technologies for Thin Crystalline Silicon Solar Cell Manufacturing (Katholieke Universiteit Leuven, Leuven, 2008).
[5] C. Boehme and G. Lucovsky, J. Vac. Sci. Technol. A **19**, 2622 (2001).
[6] V. Verlaan, Silicon Nitride at High Growth Rate Using Hot Wire Chemical Vapor Deposition (University of Utrecht, Utrecht, 2008).
[7] J. F. Lelievre, Elaboration de SiN$_x$:H par PECVD: Optimisation des Proprieties Optiques, Passivantes et Structurales pour Applications Photovoltaïques (L'Institut National des Sciences Appliquées de Lyon, Lyon, 2007), p. 80.
[8] Roth and Rau, Hohenstein-Ernstthal, Germany, "Hightech for Surfaces", accessed: October 3, 2012; http://www.roth-rau.de/.
[9] W. Soppe, H. Rieffe, and A. Weeber, Prog. Photovolt.: Res. Appl. **13**, 551 (2005).
[10] Sinton Instruments, Boulder, USA-CO, accessed: October 3, 2012; http://www.sintoninstruments.com.
[11] A. Cuevas and D. Macdonald, Sol. Energy **76**, 255 (2004).
[12] F. Giorgis, F. Giuliani, C. F. Pirri, E. Tresso, C. Summonte, R. Rizzolli, R. Galloni, A. Desalvo, and E. Rava, Philos. Mag. B **70**, 925 (1998).
[13] E. Bustarret, M. Bensouda, M. C. Habrard, J. C. Bruyère, S. Poulin, and S. C. Gujrathi, Phys. Rev. B **38**, 8171 (1988).
[14] S. Garcia, D. Bravo, M. Fernandez, I. Martil, and F. J. López, Appl. Phys. Lett. **67**, 3265 (1995).
[15] J. Robertson, Philos. Mag. B **69**, 307 (1994).
[16] A. F. Stassen, J. Anker, P. Danzl, Y. Komatsu, M. Koppes, and E. Kossen, in: Proc. 25th European Photovoltaic Solar Energy Conference and Exhibition, Valencia, Spain, 2010.
[17] D. E. Aspnes, Am. J. Phys. **50**, 704 (1982).
[18] W. L. Warren, P. M. Lenahan, and J. Kanicki, J. Appl. Phys. **70**, 2220 (1991).
[19] M. W. P. E. Lamers, K. Butler, J. Harding, and A. W. Weeber, Sol. Energy Mater. Sol. Cells **106**, 17 (2012).
[20] S. Wolf, J. Appl. Phys. **97**, 063303 (2005).
[21] M. W. P. E. Lamers, K. Butler, I. G. Romijn, J. Harding, and A. W. Weeber, in: Proc. Materials Research Society Fall Meeting, Boston, USA, 2011, pp. 1423–1428.
[22] F. de Brito Mota, J. F. Justo, and A. Fazzio, J. Appl. Phys. **86**, 1843 (1999).
[23] J. Tersoff, Phys. Rev. Lett. **56**, 632 (1986).
[24] K. T. Butler, M. W. P. E. Lamers, A. W. Weeber, and J. H. Harding, J. Appl. Phys. **110**, 124905 (2011).
[25] K. T. Butler, M. W. P. E. Lamers, A. W. Weeber, J. H. Harding, J. Appl. Phys. **112**, 094303 (2012).
[26] P. Grunow and S. Krauter, in: Proc. of the 4th IEEE World Conference of Photovoltaic Energy Conversion, Hawaii, USA, 2006, p. 2152.
[27] M. H. Kang, K. Ryu, A. Upadhyaya, and A. Rohatgi, Prog. Photovolt. **19**, 983 (2011).
[28] D. Macdonald, A. Cuevas, A. Kinomura, Y. Nakano, and L. J. Geerligs, J. Appl. Phys. **97**, 033523 (2005).
[29] C. Boehme and G. Lucovsky, J. Appl. Phys. **88**, 6055 (2000).
[30] A. Cuevas, P. A. Basore, G. GiroultMatlakowski, and C. Dubois, J. Appl. Phys. **80**, 3370 (1996).
[31] P. A. Basore and D. A. Clugston, in: Proc. 25th IEEE Photovoltiac Specialists Conference, Washington, USA-DC, 1996, p. 377.

© 2012 WILEY-VCH Verlag GmbH & Co. KGaA, Weinheim